3

Plastic deformation and fracture processes in bulk nanotwinned materials and nanotwinned nanowires

Ilya A. Ovid'ko[1,2] and Alexander G. Sheinerman[1,2]

[1]Research Laboratory for Mechanics of New Nanomaterials, St. Petersburg Polytechnical University, St. Petersburg 195251, Russia
[2]Department of Mathematics and Mechanics, St. Petersburg State University, St. Petersburg 198504, Russia

Outline:

Introduction

Nanomaterials represent a class of advanced engineering materials whose mechanical properties are often superior to those of their coarse structured counterparts. One of the most exciting properties of nanomaterials is that they frequently demonstrate very high strength but commonly at the expense of low ductility. Recently, however, nanomaterials have been fabricated that show a combination of ultrahigh yield strength and high ductility [1–4]. Such solids, called nanotwinned materials, represent ultrafine-grained materials containing layered growth nanotwins. The fabrication of nanotwinned materials provides the opportunities of governing the mechanical and functional properties of nanomaterials via tuning the twin thickness and geometry of coherent twin boundaries. These materials also represent an interesting model system, since their deformation can be realized through deformation mechanisms that are not observed in other kinds of crystalline solids.

In this chapter, we give a review of experiments, molecular dynamics simulations and theoretical modeling concerning the mechanisms of plastic deformation and fracture of nanotwinned solids. We consider the mechanisms of their strengthening and toughening, examine the experiments and computer simulations dealing with their exceptionally high strength, touch on the models describing the anomalous dependence of their yield strength on twin thickness and discuss the effects of texture and plastic anisotropy on the mechanical characteristics of textured nanotwinned solids. We also review the results of the experiments, simulations and modeling concerning failure of nanotwinned solids, with a focus on brittle-to-ductile transition observed either with a decrease or with an increase of twin thickness. Besides, we consider the results of experiments and simulations concerning plastic deformation and fracture of nanotwinned nanowires.

Strength of bulk nanotwinned materials

Bulk nanotwinned materials represent bulk polycrystalline solids where submicrocrystalline or microcrystalline grains consist of growth twins of nanoscopic thickness [1–35] (Fig. 3.1). Nanotwinned solids are commonly fabricated via electrodeposition [1–3] or physical vapor deposition [36–39], and the average twin thickness decreases with increasing electrodeposition rate [2]. Direct electron microscopy observations of nanotwinned materials demonstrate that twins in such materials, although differ in thickness, form relatively regular structures [4,8,13,40] (Fig. 3.1). Strength and hardness of such materials significantly exceed the corresponding characteristics of nanocrystalline materials with the same composition (for example, nanotwinned diamond can have unprecedented microhardness of 200 GPa [11]) while their strain to failure is 3 to 10 times as high as that of similar nanocrystalline solids (e.g., [2]).

These extraordinary properties of nanotwinned solids are attributed to the interactions of dislocations with twin boundaries [4]. In face centred cubic (fcc) nanotwinned solids these are coherent twin boundaries. The nanoscale spacing between adjacent coherent twin boundaries restricts dislocation motion within the twin lamellae and prevents the formation of dislocation pileups in the interiors of such lamellae. To carry plastic deformation, dislocations must transfer across the twin boundaries. In the case of fcc nanotwinned solids, the misorientation angle between the {111}<110> slip planes in adjacent twin lamellae is high, which creates a very high barrier for individual dislocation transmission across a twin boundary and results in high strength of nanotwinned solids.

One should note that in nanotwinned solids, the dependence of yield strength on the average twin lamellae thickness has a complicated character. Experiments and molecular dynamics (MD) simulations demonstrate that the yield strength of nanotwinned metals (made by electrodeposition) with fcc crystal lattices decreases with increasing twin thickness above some critical twin thickness and increases with twin thickness if twin thickness is below this critical value (see, e.g., [2,6,7] and references therein) (Fig. 3.2). (This softening behaviour does not occur for fibre-textured nanotwinned metals fabricated by sputtering [41].) Such mechanical behaviour of nanotwinned solids resembles the anomalous dependence of yield strength on grain size in nanocrystalline materials. The change in the character of the dependence of yield strength on twin thickness in nanotwinned solids when passing to small twin thicknesses is attributed to a change of plastic deformation mechanism in such solids. For large enough twin thicknesses, plastic deformation is realized through the motion of dislocations from one twin boundary to another. However, at sufficiently small twin thicknesses, when the stress needed to emit a dislocation from a twin boundary becomes very high, the transition in the plastic deformation mechanism occurs. In the latter case, plastic deformation is realized through the emission of partial Shockley dislocations from the junctions of grain and twin boundaries followed by their motion over twin boundaries across the grain and absorption by the opposite grain boundary [6,9,10,15]. These two deformation mechanisms have been observed experimentally in nanotwinned metals with equiaxed grains and in nanotwinned nanowires [42,43].

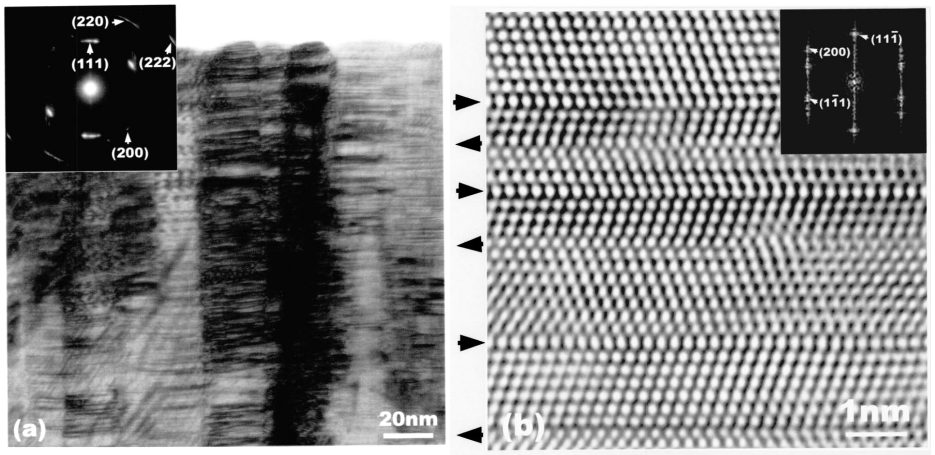

FIGURE 3.1
(a) Bright field transmission electron microscopy (TEM) image of 330 stainless steel films showing high density twinning within the columnar grains. (b) High resolution TEM image showing nanoscale growth twins in sputtered 330 stainless steel films, with arrows indicating twin interfaces. Reproduced from [37], with permission. Copyright 2004, AIP Publishing LLC

To describe the yield strength of nanotwinned metals below the critical twin thickness, Li et al. [6] suggested a simple kinetic model describing emission of Shockley partials from the junctions of twin and grain boundaries. Within their model, such dislocation emission occurs under the action of the resolved shear stress and is assisted by the stress concentration at the junctions of twin and grain boundaries and thermal fluctuations. They suggested the following formula for the shear yield strength of the nanotwinned solid τ_y :

$$\tau_y = \frac{\Delta U}{SV^*} - \frac{k_B T}{SV^*} \ln\left(\frac{d}{\lambda}\frac{\nu_D}{\dot{\varepsilon}}\right), \qquad (1)$$

where ΔU is the activation energy, S is a factor representing local stress concentration and geometry, λ is the twin thickness, d is grain size, V^* is the activation volume, k_B and T are the Boltzmann constant and temperature, ν_D is the Debye frequency, and $\dot{\varepsilon}$ is the macroscopic strain rate. For a given grain size d, formula (1) predicts that τ_y decreases with decreasing twin thickness λ, which is related to a higher number of potential sites (at the junctions of grain and twin boundaries) for Shockley dislocation emission.

Figure 3.2 shows a comparison of the yield stress of nanotwinned ultrafine-grained Cu from experimental data, the model predictions based on equation (1) and MD simulations. The softening behaviour seen in the simulations below the critical twin boundary spacing is well captured by formula (1). For a given grain size d, the intersection of the curve obtained from equation (1) and the Hall–Petch relation indicates where the onset of strength softening occurs in a nanotwinned metal, provided that the Hall–Petch relation remains valid for twin-boundary spacing as small as several nanometers. As shown in Fig. 3.2, simulations and formula (1) show that the onset of softening depends on the grain size: the smaller the grain size d, the smaller the critical twin boundary spacing, and the higher the maximum strength of the material.

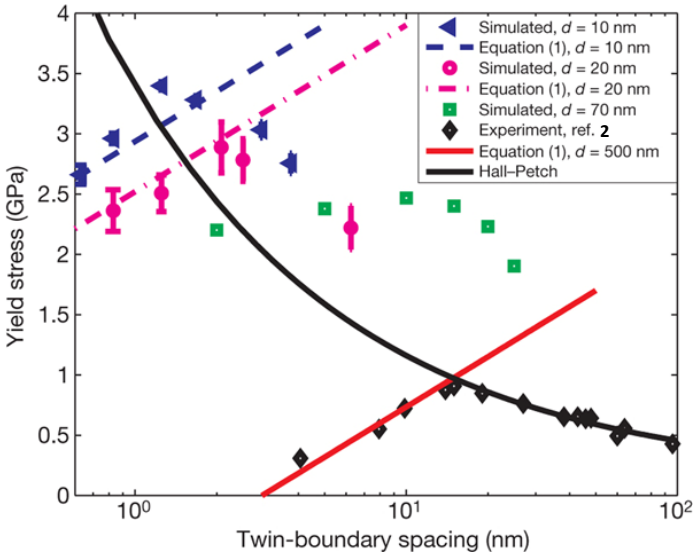

FIGURE 3.2
Yield stress of nanotwinned Cu as a function of twin-boundary spacing at different grain sizes. Experimental data in the strength increasing region is fitted to the Hall–Petch equation. MD simulation results (symbols) for yield stress for *d*=10 nm, 20 nm and experimental data for *d*=500 nm, are shown together with the corresponding fitted curves from equation (1). The quasi-three-dimensional simulation results for *d*=70 nm are shown but not fitted because equation (1) is based on dislocation nucleation in three-dimensional nanotwinned metals. Adapted from [6], with permission. Copyright 2010, Nature Publishing Group

Wang et al. [44] suggested another model for softening of nanotwinned materials at small twin thicknesses. In their MD simulations they observed collective glide of partial dislocations. They assumed, therefore, that at small twin thicknesses, plastic deformation is realized via detwinning

occurring through the collective glide of walls of partial dislocations. Wu et al. [45] supposed that above the critical twin thickness, plastic deformation occurs via cross-slip and dissociation of Lomer dislocations. Dissociating dislocations hinder further dislocation motion, thus increasing the yield stress. At the same time, at sufficiently small twin thicknesses (below the critical value), cross-slip does not occur, and instead steps form on the twin boundaries. These steps then move and serve as dislocation nucleation sites, softening the material.

Ovid'ko and Skiba [46] assumed that nanotwinned materials with growth twins contain rotational defects – wedge disclinations – at the junctions of twin and grain boundaries (Fig. 3.3) similar to those formed at the junctions of twin and grain boundaries during the formation of deformation twins. Within their model, pre-existent wedge disclinations hinder the emission and motion of Shockley partial dislocations occurring at small twin thicknesses, and their hindering effect is the stronger, the higher is twin thickness. This explains the decrease of the yield strength with decreasing twin thickness at small twin thicknesses.

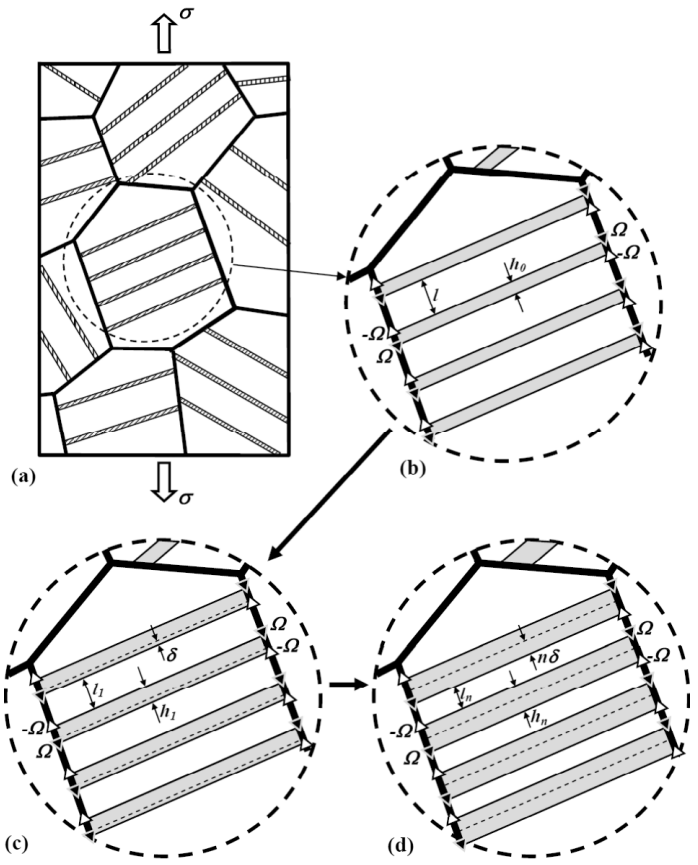

FIGURE 3.3

Plastic flow in a nanotwinned metal specimen occurs through motion of twin boundaries and is accompanied by evolution of disclinations (shown by triangles). (a) A nanotwinned metal specimen is under a tensile load (general view). (b) The typical model grain contains *N* periodically arranged identical nanotwins. (c,d) Plastic deformation occurs through motion of twinning partials and is accompanied by motion of both twin boundaries and disclinations. Reprinted from [46], with permission. Copyright 2014, Advanced Study Center

Stukowski et al. [7] performed large-scale MD simulations of uniaxial tensile deformation of nanotwinned Cu and Pd. Their MD simulations demonstrated an interesting feature: whereas the yield and flow stresses of the model nanotwinned Cu specimen were higher than those of a similar twin-free Cu specimen, the yield and flow stresses of model nanotwinned Pd were lower than those of a similar twin-free Pd specimen (Fig. 3.4). Detailed study of deformation mechanisms in Cu and Pd revealed that various deformation mechanisms act in nanotwinned Cu, namely twin boundary migration, emission of partial or perfect lattice dislocations from the grain boundaries, formation of extrinsic stacking faults, and interaction of partial dislocations with twin boundaries. At the same time, nanotwinned Pd deforms almost exclusively via twin boundary migration. Irrespective of the local grain and twin boundary orientation, twinning dislocations nucleate on glide planes parallel and adjacent to twin boundaries. At sufficiently small twin thicknesses, the stress for twin boundary motion in nanotwinned Pd appears to be smaller than the stress for dislocation emission from grain boundaries (or other grain boundary mediated deformation mechanisms) in twin-free Pd. This explains the lower yield and flow stresses of nanotwinned Pd compared to the similar twin-free Pd specimen.

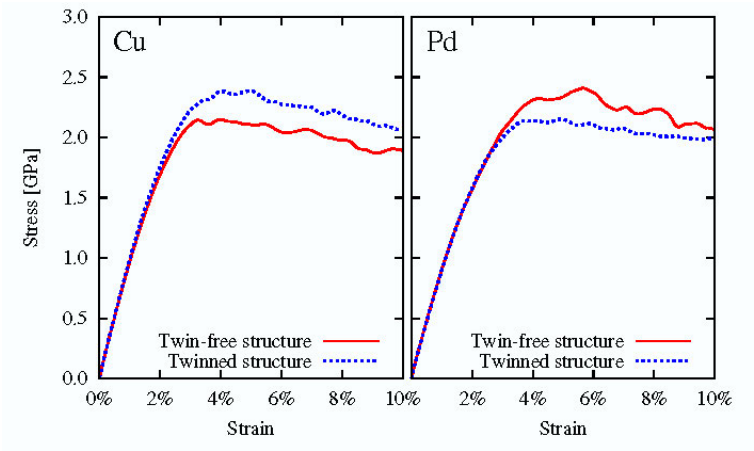

FIGURE 3.4
Stress-strain curves obtained for uniaxial tensile deformation of nanocrystalline Cu and Pd. For each element, two different structures were tested: a defect-free microstructure with 20 nm grain size and an identical structure containing growth twins (4 nm spacing). The simulated strain rate was 10^8 s^{-1}. Reproduced from [7], with permission. Copyright 2010, American Physical Society

Plastic deformation processes in columnar-grained nanotwinned solids

Recently, nanotwinned metals with elongated cylindrical grains have been obtained via direct electrodeposition [9,39,47]. Such samples have pronounced texture, and their twin boundaries are primarily located normally to the axes of cylindrical grains [9,47]. It was found that Cu samples with elongated grains are characterized by essential plastic anisotropy and high resistance to fatigue fracture, since their deformation behaviour strongly depends on the thickness and orientation of twin boundaries [9].

In particular, for the case where the tensile load direction is parallel to twin boundary planes and the twin thickness is sufficiently small, Zhou et al. [15], using MD simulations, have revealed a transition in the deformation mechanism with a decrease in twin thickness. At sufficiently large twin thicknesses, plastic deformation is realized through the formation and expansion of isolated dislocation loops embedded in individual twin lamellas (Fig. 3.10). Each such dislocation loop incorporates two horizontal segments on the neighboring twin planes and threading segments, one of which is spanning across the twin lamella. The threading segment moves from one GB to another under the action of a resolved shear stress, and this process is accompanied by an extension of dislocation segments lying at twin boundaries (Fig. 3.5). However, at sufficiently small twin thicknesses, the large energy associated with the horizontal loop segments at twin boundaries make the formation of such extended dislocation loops unfavored, and the deformation mechanism switches to the formation and motion of jogged dislocations (Fig. 3.5). Every jogged dislocation is composed of moving threading segments (jogs) in between twin boundaries and penetrates multiple twins. Also, a jogged dislocation is a split one and comprises two partial dislocations (each threading multiple twins) divided by a stacking fault. The line of the resulting split dislocation resembles a necklace (Fig. 3.5), so that the dislocation is also called a necklace dislocation. The formation of a necklace dislocation can be favoured at small twin thickness (below 2-5 nm), when the critical stress for the depinning of unit jogs of a jogged dislocation becomes smaller than that for the expansion of an extended dislocation loop inside an individual twin lamella.

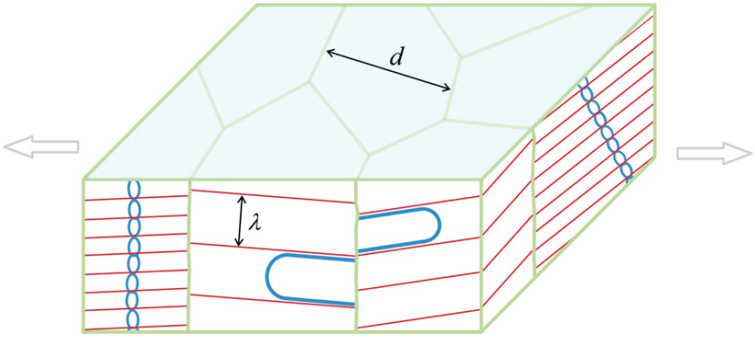

FIGURE 3.5
Deformation mechanisms in fibre-textured nanotwinned materials for the case where the applied load direction is parallel to twin boundary planes. In columnar grains with small twin thicknesses, deformation occurs through the motion of the threading segments of a jogged necklace-like dislocation (under the action of a resolved shear stress). In columnar grains with large twin thicknesses, deformation occurs through the motion of threading segments of extended dislocation loops embedded in individual twin lamellas. In the latter case, the motion of the threading segments is accompanied by the extension of the dislocation segments located at twin boundaries. Reproduced from [15], with permission. Copyright 2014, American Chemical Society

You et al. [9] studied anisotropic plastic deformation in columnar-grained copper containing preferentially oriented nanoscale twins by experimental testing, crystal plasticity modelling and MD simulations. It appeared that the yield strength and flow stress are highest when the compression axis is normal to the twin boundary planes, become smaller when twin boundaries are parallel to the compression axis, and are lowest if twin boundary planes make an angle of 45° with the compression axis. They also revealed that in the first two cases (where twin boundary planes are

normal or parallel to the compression axis) strain hardening is small, while in the latter case (where twin boundary planes make an angle of 45° with the compression axis) strain hardening is pronounced. The different deformation behaviours were attributed to different deformation mechanisms acting in the examined three cases. In the first case (where twin boundary planes are normal to the compression axis), deformation occurs via dislocation transfer across twin boundaries. In the second case (where twin boundary planes are parallel to the compression axis), deformation is realized via the motion of jogged dislocations in between the twins. In the last case, where twin boundary planes make an angle of 45° with the compression axis, deformation is realized through Shockley dislocation motion over twin boundaries. Thus, the controllable switching of deformation mechanisms not only leads to a pronounced dependence of yield strength on loading orientation, but also induces a strong orientation dependence of strain hardening.

Plastic deformation of twinned nanowires

Along with bulk nanotwinned solids, last years nanotwinned nanowires attracted much attention as good candidates for the use in electronic materials (e.g., [48–50]). In particular, recently Chen et al. [51] fabricated dense arrays of nanotwinned Cu nanowires, where the presence of twin boundaries dramatically increased the critical current density. Also, nanotwinned nanowires with high-density twins demonstrate extremely high strength (close to the theoretical strength limit [52,53]). All that motivated intensive studies of plastic deformation and fracture mechanisms in nanotwinned nanowires.

Deng and Sansoz [54,55] performed large-scale MD simulations of dislocation nucleation in circular [54] and faceted [55] twinned gold nanowires (containing twin boundaries normal to the nanowire axis) under tensile loading. They found that the critical resolved shear stress τ_c for dislocation nucleation scales linearly with the inverse of the twin thickness $1/h$, and the slope of the linear dependence of the critical stress τ_c on $1/h$ increases with decreasing the nanowire diameter (Fig. 3.6). They also revealed that the addition of nanoscale twins to crystalline nanowires can either increase or decrease the critical stress for dislocation nucleation, depending on both sample diameter and twin thickness. An increase of the critical stress τ_c for dislocation nucleation with increasing twin density $1/h$ is intuitively clear, since twin boundaries serve as barriers for dislocation propagation and can stop dislocations close to the free surface, where they are subjected to a strong image force exerted by the free surface. At the same time, the reason for a decrease of the critical stress for dislocation nucleation for twinned nanowires with large twin thickness compared to the critical stress for single-crystalline, twin-free nanowires is not quite clear. Presumably, this can be associated with the difference in dislocation slip planes in the cases of twinned and twin-free nanowires.

Wang et al. [53] studied the critical tensile strain for dislocation nucleation in nanotwinned [111]-oriented gold nanowires under tension using *in-situ* high-resolution transmission electron microscopy (TEM). Interestingly, they obtained a strong Hall-Petch type relationship of the critical tensile strain on twin thickness up to strain of 5.3%, or near the ideal theoretical limit, as the twin size is decreased below 3 nm (Fig. 3.7). Based on the results of previous MD simulations, Wang et al. [53] concluded that as the twin size decreases below 2.8 nm, the critical strain for dislocation nucleation converges asymptotically to the ideal theoretical limit of 5.5% without a significant change of the twin thickness. Wang et al. [53] attributed this to a change of dislocation formation

mechanism from heterogeneous nucleation from the free surface to homogeneous nucleation in the limited space between twin boundaries inside the nanowire [52].

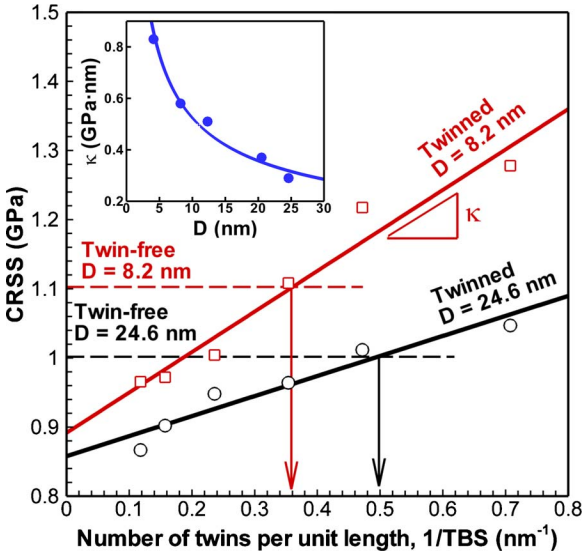

FIGURE 3.6
Change in the critical resolved shear stress (CRSS) for dislocation nucleation as a function of the number of twin boundaries per unit length, 1/TBS, in simulated gold nanowires with diameters equal to 8.2 and 24.6 nm at 300 K. A mechanical transition from twin-induced weakening to strengthening regimes is indicated by a vertical arrow. The inset shows the change in the slope of the fitted line as a function of nanowire diameter *D* varying from 4.1 to 24.6 nm. Reproduced from [54], with permission. Copyright 2009, American Institute of Physics

Wu et al. [56] performed MD simulations to identify the relevant yield mechanisms for both single-crystalline and nanocrystalline nanotwinned Cu nanowires. By characterizing the deformation at the yield point on the atomic scale, they observed that the initial yields in all nanowires occur via dislocation nucleation from surfaces or surface defects (for single-crystalline nanotwinned nanowires) and from grain boundary triple junctions for nanocrystalline nanotwinned nanowires. They observed that both surface defects in single-crystalline nanotwinned nanowires and grain boundary triple junctions in nanocrystalline nanotwinned nanowires act as effective stress concentrators that promote dislocation nucleation. However, the higher density of triple junctions in nanocrystalline nanotwinned nanowires makes these structures considerably weaker than their single-crystalline nanotwinned counterparts. Also, the simulations demonstrated that in contrast to the case of single-crystalline nanotwinned nanowires, the presence of nanotwins in nanocrystalline Cu nanowires very weakly increases the nanowire yield strength. However, the reason for this behaviour is not quite clear yet.

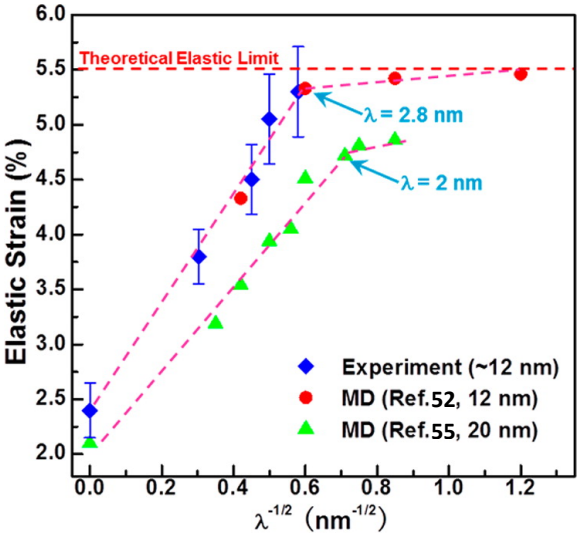

FIGURE 3.7

The critical strain for dislocation formation in nanotwinned [111]-Au nanowires vs. $\lambda^{-1/2}$, where λ is the twin thickness. The red dots represent the MD simulation data from ref. [52] with the nanowire diameter of 12 nm; while the green triangles represent the MD simulation data from ref. [55] with the nanowire diameter of 20 nm. Both experiment and simulation results show that for twin thicknesses larger than 3 nm, the critical strain for dislocation nucleation can be linearly related to $\lambda^{-1/2}$, suggesting a strong Hall–Petch type hardening. Near ideal elastic strain limit is achieved as the twin size decreases below 2.8 nm. Adapted from [53], with permission. Copyright 2015, American Chemical Society

Fracture of bulk nanotwinned solids

Now let us consider crack propagation and fracture of nanotwinned materials. Liu et al. [57] studied in situ crack propagation in nanotwinned Ag using a high resolution transmission electron microscope (HRTEM). They observed that the dynamic processes of crack penetration across the coherent twin boundaries involve alternated crack tip blunting, crack deflection, twinning/detwinning and slip transmission across the twin boundaries. The alternated blunting processes were related to the emission of different types of dislocations at the crack tip and varied with the distance of the crack tip from the coherent twin boundaries. It appeared that the crack tip sharpens as the crack approaches the coherent twin boundary, which is explained by suppression of some slip systems near the twin boundary.

In order to understand the above plastic and fracture processes, Liu et al. [57] conducted MD simulation for nanotwinned silver (Fig. 3.8). The simulations demonstrated the emission of an extended full dislocation from the crack tip (Fig. 3.8a) followed by its glide towards the nearest twin boundary, dislocation reaction at the boundary and dislocation transmission across the boundary. At the same time, when the crack tip is at some short distance from the nearest twin boundary (Fig. 3.8a), the crack tip is not blunted efficiently (Fig. 3.8a,b). However, when the crack tip approaches the twin boundary, the slips along the twin boundary are further enhanced (Fig. 3.8c) and the crack is blunted more intensely. As a result, the blunted crack tip slows down crack propagation. At the same time, the slips of Shockley partials along the twin boundary lead to twin boundary migration until the two twins on the right part are merged. As a result, the slip system for the slip of Shockley

partials is deactivated, and the crack tip is sharp again during the subsequent propagation (Fig. 3.8d). Thus, the crack tip can be blunted more efficiently if it is adjacent to the twin boundary.

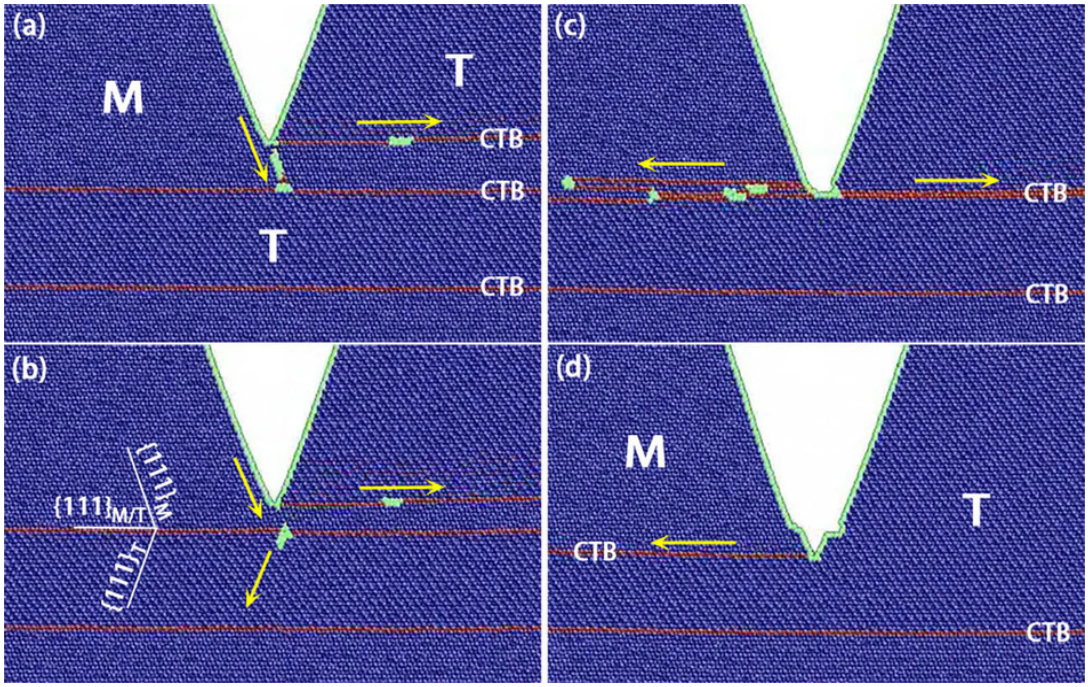

FIGURE 3.8
MD simulation of the cracking of nanotwinned Ag. Shockley partial dislocations are emitted from the crack tip and glide towards the right in (a, b) before the crack penetrates the coherent twin boundary, and towards the left in (c, d) after the penetration across the twin boundary. A full dislocation is emitted from crack tip in (a), is blocked at the twin boundary and transfers into the twin in (b). More partials are emitted and the crack tip is blunted in (c). The crack tip becomes sharp again when close to the next twin boundary in (d). The yellow arrows indicate the gliding directions. ''M'' and ''T'' mean matrix and twin, respectively. Reprinted by permission from Macmillan Publishers Ltd: Scientific Reports (ref. [57]), copyright (2014)

Zhou et al. [58] studied crack propagation in nanotwinned Ni using MD simulations. They revealed the following four toughening mechanisms associated with twin boundaries: (i) crack blunting through dislocation emission from the crack tip along the twin boundaries; (ii) crack deflection toward an intragranular path; shielding by the nucleation and growth of daughter cracks and (iv) curving of the nanoscale twin boundaries due to an excessive pileup of partial dislocations (Fig. 3.9). Using MD simulations, Zhou et al. [58] also calculated the fracture toughness of nanotwinned Ni and concluded that twin boundaries increase fracture toughness by 10 to 50%.

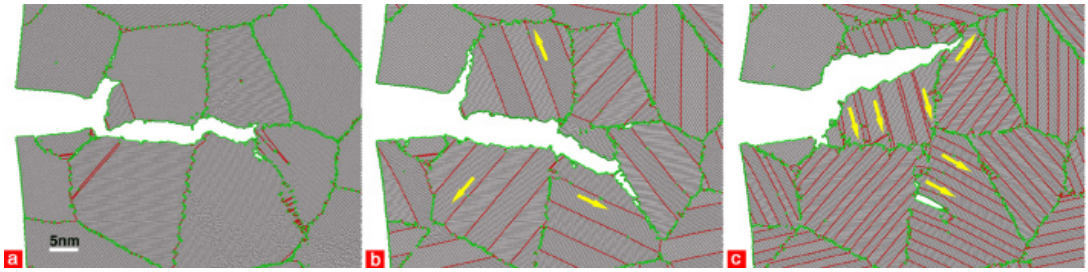

FIGURE 3.9
Dislocation accommodation and crack deflection. Dislocation core atoms and atoms on the crack surfaces are coloured green, as well as grain boundary atoms. Atoms representing stacking faults are coloured red. The yellow arrows indicate the sliding of partial dislocations along the twin boundaries. (a) Crack propagation in a model sample without twin boundaries. The crack takes an intergranular path, inducing scarce dislocation activities. (b) Crack propagation in the model sample with a twin boundary spacing of 5 nm. The crack begins an intragranular path that transects the second grain. Movements of dislocations along the twin boundaries are clearly visible. (c) Crack propagation in the model sample with a twin boundary spacing of 2 nm. The crack begins an intragranular path, leading to a large number of dislocations emitted along the twin boundaries. Reproduced from [58] (doi:/10.1088/0965-0393/18/6/065002), with permission.

Hodge et al. [8] studied and compared deformation behaviour of nanotwinned Cu with grain size of 500 to 800 nm and low twin density at room temperature and at a low temperature of 77 K. They observed that at low temperature nanotwinned Cu has strength (maximum achievable stress) of 700 MPa, which is higher than that (around 500 MPa) at room temperature. Besides, the specimens at low temperature demonstrated higher strain to failure (around 11%) that at room temperature (approximately 8%). The observation demonstrated that in both cases, the specimen fails due to necking, which is associated with the formation of shear bands. The higher strength observed at liquid nitrogen temperature was clear enough, since dislocations move slower at 77 K and there is a general lack of mobile dislocations. However, the reasons for increasing ductility at 77 K are not yet clear.

Sinha and Kulkarni [59] studied crack propagation along coherent twin boundaries in nanotwinned metals using MD simulations. They revealed that alternating twin boundaries exhibit intrinsic brittleness and ductility due to the opposite crystallographic orientations of the adjoining twins. They considered the evolution of the atomically sharp crack on positive and negative coherent twin boundaries, respectively, in a nanotwinned specimen under mode I loading (Fig. 3.10). When the crack is on a “positive” twin boundary, it propagates via cleavage along the twin boundary. However, when the crack is located on an adjacent (“negative”) twin boundary, it favours dislocation emission from the crack tip. The analytical calculations performed by Sinha and Kulkarni [59] demonstrated that the intrinsic brittleness of “positive” twin boundaries is related to the absence of favourably oriented planes for dislocation emission from the crack tip. As a result, the cleavage becomes more energetically favourable that dislocation emission. At the same time, MD simulation performed for the case of an initially blunted crack demonstrated that blunting of the sharp crack by insertion even one atomic half-layer makes it intrinsically ductile. Thus, blunting a crack tip even by an atomic layer can cause a brittle-to-ductile transition by making it easier to emit a dislocation.

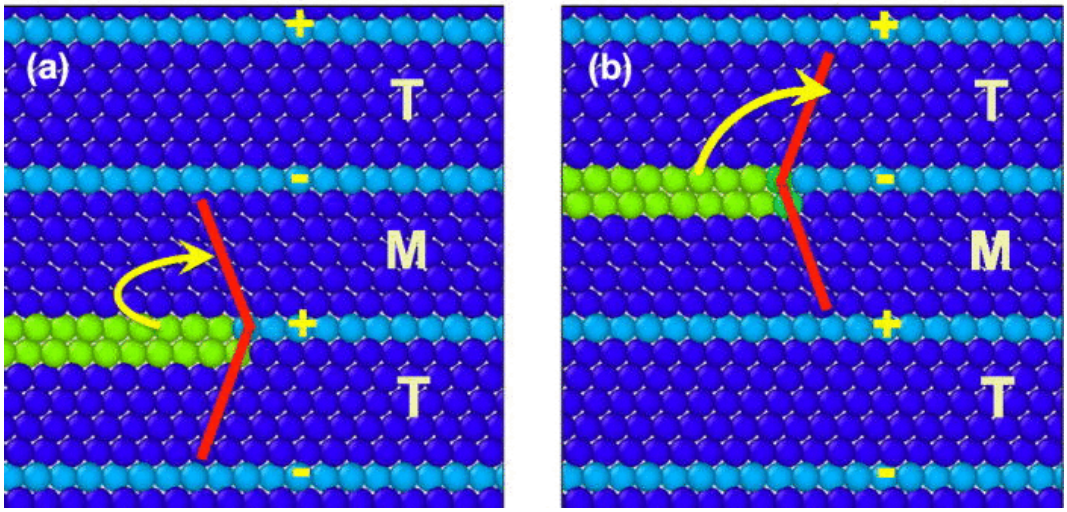

FIGURE 3.10
(a) Crack located on a "+" coherent twin boundary with matrix "M" orientation above and twin "T" orientation below. (b) Crack located on a "–" coherent twin boundary with "T" orientation above and "M" orientation below. The red lines mark the projections of the {111} planes in the matrix and the twin. The atoms on the crack are shown in green, the twin boundary atoms are shown in light blue, and the fcc atoms are shown in dark blue colour. Reprinted with permission from [59]. Copyright 2014, AIP Publishing LLC

Fracture of twinned nanowires

Intrinsic brittleness of coherent twin boundaries in nanotwinned solids, discussed in the previous section, gives rise to interesting ductile/brittle behaviours and ductile-to-brittle transitions in nanotwinned nanopillars/nanowires. For example, Jang et al. [43] experimentally observed a ductile-to-brittle transition in copper nanopillars (containing twin boundaries normal to the nanopillar axis) under tension with increasing twin thickness above 2.8 nm.
To explain this effect, Jang et al. [43] performed MD simulations of crack propagation in nanopillars along twin boundaries. It appeared that due to the intrinsic brittleness of the coherent twin boundaries, discussed above, for not too small twin thicknesses (4.38 nm or larger) the crack propagates in a brittle fashion, without any plastic deformation. However, at very small twin thickness (1.25 nm or smaller) a new toughening mechanism is activated (Fig. 3.11). This mechanism represents the homogeneous generation and expansion of dipoles of Shockley partials at twin boundaries adjacent to the crack tip. The generation of such dipoles is followed by dislocation emission from the crack tip and crack blunting. Eventually, the sample fails due to necking.
To estimate the critical twin thickness for the ductile-to brittle transition, Jang et al. [43] suggested a theoretical model for the homogeneous nucleation of a Shockley dislocation dipole near the crack tip in a nanotwinned nanopillar/nanowire under tension. They assumed that (i) to generate a dislocation dipole near the crack tip, the applied load should be smaller than that for crack propagation and (ii) the critical resolved shear stress (for Shockley dislocation dipole nucleation) should be equal to the shear cohesive strength of the solid. Using this model, for the case of Cu,

they derived the critical twin thickness to be equal to 2.37 nm, which agrees well with the results of experiments and MD simulations. Thus, the results of paper [43] demonstrated that the ductile-to brittle transition in twinned nanopillars/nanowires is associated with the formation of the dipoles of Shockley partials at twin boundaries near the crack tip at small enough twin thicknesses.

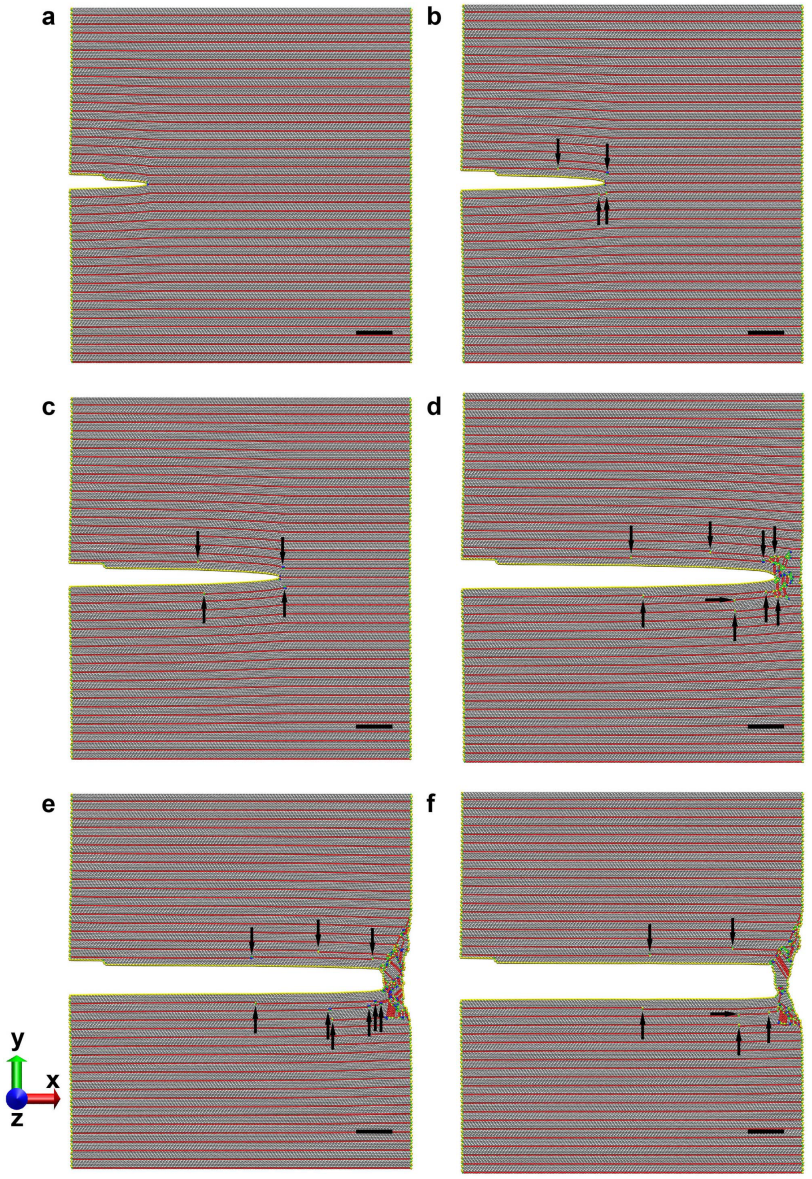

FIGURE 3.11

Snapshots of crack propagation in nanotwinned Cu with twin boundary spacing of 1.25 nm at different strains. (a) $\varepsilon = 3.56\%$ (b) $\varepsilon = 4.60\%$. (c) $\varepsilon = 5.65\%$. (d) $\varepsilon = 7.79\%$. (e) $\varepsilon = 9.42\%$. (f) $\varepsilon = 11.18\%$. During crack propagation, twinning dislocations first nucleate on twin boundaries near the crack tip, followed by dislocation emission from the crack tip and crack blunting. Eventually, the sample fails due to necking. Twinning dislocations are indicated by black arrows. The scale bars are 5 nm. Reprinted by permission from Macmillan Publishers Ltd: [Nature Nanotechnology] (ref. [43]), copyright (2012)

While Jang et al. [43] observed a ductile-to-brittle transition in copper nanopillars with increasing twin thickness above 2.8 nm, Wang et al. [52] experimentally revealed an opposite effect: ductile-to-brittle transition in gold nanowires with decreasing twin thickness below 2.8 nm. As in the experiment of Jang et al. [43], Wang et al. [52] studied tensile behaviour of nanowires containing twins whose planes are normal to the nanowire axis. To do so, they synthesized gold nanowires with ultradense twins (with the twin thickness as small as 0.7 nm) as well as nanowires with low-density twins and those with bimodal twin thickness distribution (containing both ultradense twins and low-density twins).

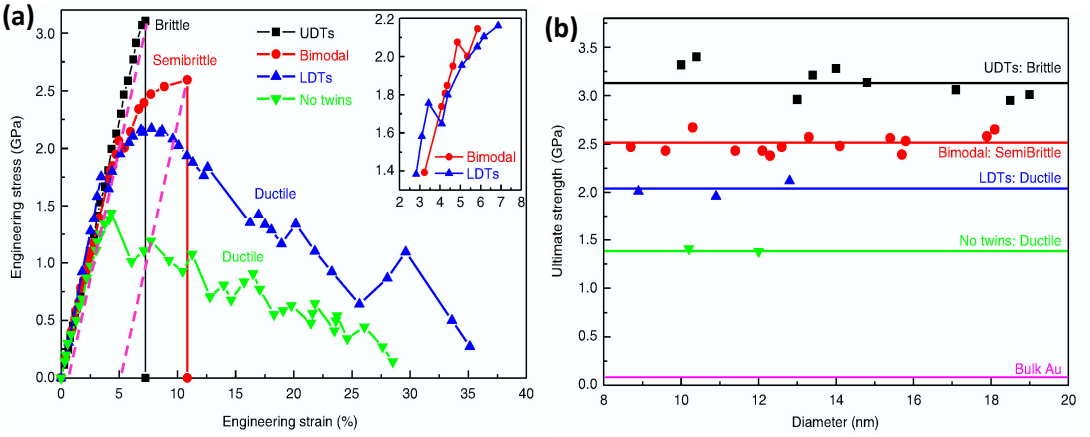

FIGURE 3.12
(a) Representative stress–strain curves for Au nanowires with different structures obtained by in-situ TEM–AFM experiments. Dash lines in pink colour indicate the permanent inelastic deformation after fracture. The diameters of samples with either ultradense twins or bimodal structures are almost identical, 14.5 and 13.4 nm respectively. The inset shows a close-up view of the yield points in the specimens with bimodal and low-density twins. (b) Strength distribution in Au nanowires with different fracture modes. Reprinted by permission from Macmillan Publishers Ltd: [Nature Communications] (ref. [52]), copyright (2013)

The mechanical properties of ultratwinned Au nanowires studied by Wang et al. [52] under tensile loading are shown in Fig. 3.12. Figure 3.12 shows that the mechanical response of Au nanowires with ultradense twins differs markedly from that of Au nanowires with low-density twins and without twins. The ultimate strength of twin-free Au nanowires was found to be equal to 1.43 GPa with no strain hardening after yielding. The mechanical response of Au nanowires with low-density twins is characterized by significant strain hardening with an ultimate strength of around 2.05 GPa after yielding (around 1.7 GPa), as well as by considerable ductility (characterized by strain to failure around 35%). Figure 3.12a shows that this behaviour is in contrast to the behaviour of Au nanowires with ultradense twins, where strain hardening is absent, ductility is considerably reduced, and the elastic limit increases to 3.12 GPa (Fig. 3.12a,b), which is much higher than that of Au nanowires with low-density twins and no twins (Fig. 3.12b). This limit corresponds to a critical resolved shear stress of 0.98 GPa for partial dislocation {111}<112> slip, which is very close to the ideal shear strength of 1.42 GPa for pure Au reported from first-principle calculations [60]. Moreover, the fracture behaviour of Au nanowires with ultradense twins is brittle-like with a flat fracture surface perpendicular to the loading axis. Although the total elongation is about 7.2% due to the high elastic strain, plastic elongation at failure is very small (<1%). In contrast, the behaviour of nanowires with bimodal twin thickness distribution appears to be semibrittle with slightly lower

yield strength (around 2.1 GPa) and limited, but finite inelastic deformation (around 5%) and the ultimate stress of 2.52 GPa (Fig. 3.12a,b).

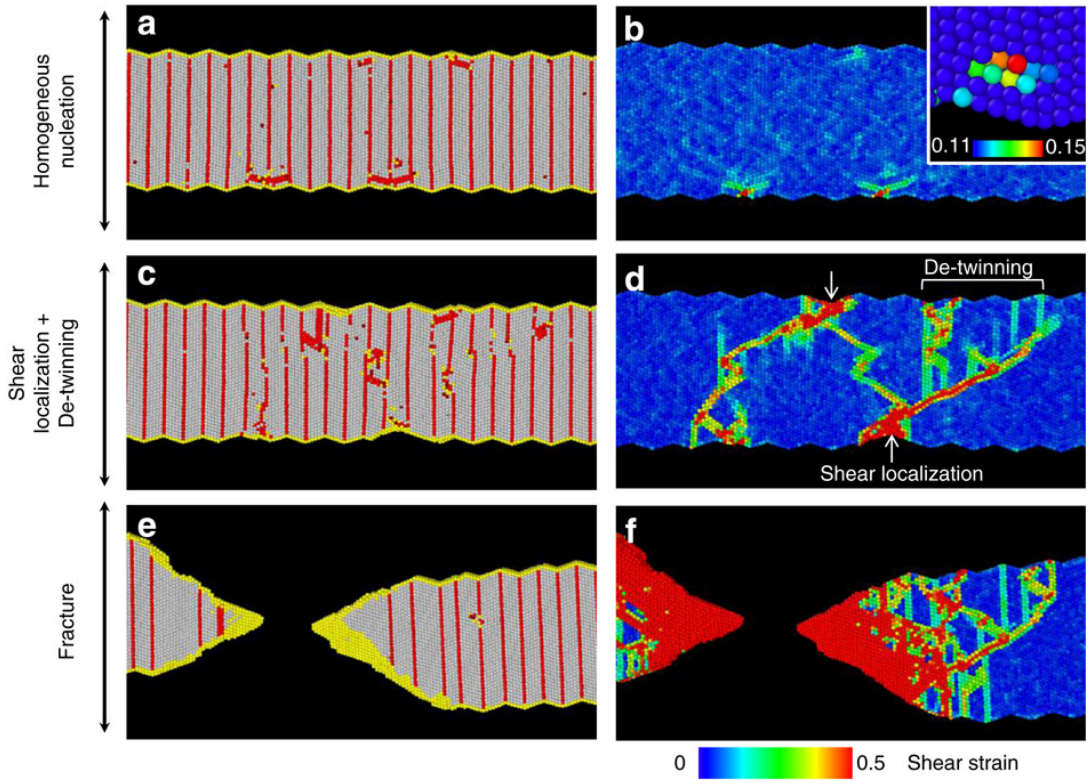

FIGURE 3.13
Simulated deformation structures (a,c,e) and shear strain (b,d,f) in a deformed brittle-like Au nanowire. The Au nanowire contains ultradense twins with twin thickness of 1.4 nm and {111} surface microfacets. (a,b) Homogenous nucleation, 5.2% strain. (c,d) Plastic shear localization and detwinning, 5.6% tensile strain. (e,f) Fracture above 5.75% strain. Reprinted by permission from Macmillan Publishers Ltd: [Nature Communications] (ref. [52]), copyright (2013)

Based on the above results, Wang et al. [52] concluded that a sharp transition from ductile plasticity to brittle fracture takes place in ultratwinned Au nanowires with increasing twin density. To clarify the nature of the ductile-to-brittle transition, they performed in-situ high resolution transmission electron microscopy (HRTEM) study of the examined nanowires as well as MD simulations of their behaviour under tensile loading. The above studies confirmed that the deformation of Au nanowires with low-density twins and no twins is dominated by dislocations nucleating from free surfaces. In the Au nanowires with low-density twins uniform plastic elongation followed by necking mainly occurs between twin boundaries with the largest twin thickness. Similarly, the MD simulations for gold nanowires with low-density twins demonstrated extensive plastic deformation carried by partial dislocations nucleating from the surface and accompanied by stacking faults.

At the same time, in-situ HRTEM observations of gold nanowires with ultradense twins (with a predominance of twins with a thickness of 0.7 nm) demonstrated considerable elastic elongation

followed by sudden failure at an applied strain of 6.8% due to necking. The fracture process occurred so fast that rare dislocation activity was observed, although significant slip and detwinning have occurred in the confined zone where necking occurs. This result was further supported by the MD simulations, where fracture was contained within a short nanowire segment exhibiting significant detwinning, as in the HRTEM experiments. Also, MD simulations demonstrated that the onset of yielding in brittle-like nanowires is due to homogeneous nucleation of dislocations between twin boundaries near nanowire free surfaces at ultrahigh stresses, in contrast to heterogeneous deformation from free surfaces. The generated dislocations create high shear stresses in the twin planes, resulting in detwinning of the fractured region followed by nanowire failure (Fig. 3.13). Thus, the study of Wang et al. [52] demonstrated that although nanowires with ultradense twins are stable with respect to twin propagation [43], they can exhibit brittle-like deformation behaviour due to very fast shear localization and necking, in contrast to nanowires with low-density twins, which, if crack-free, demonstrate slow ductile failure.

Conclusions and future outlook

In summary, nanotwinned materials possess intriguing mechanical properties, including a unique combination of ultrahigh strength with significant ductility. The excellent mechanical properties of nanotwinned materials are partly associated with elongated geometry of twins, which hinder dislocation motion across grains along most favourable crystallographic planes, thus providing high strength of nanotwinned materials, but, at the same time allow massive dislocation emission from crack tips along coherent twin boundaries, thereby providing good toughness of nanotwinned solids. Also, plastic deformation in nanotwinned solids can be realized by a variety of deformation mechanisms, including twin boundary migration, emission of partial or perfect lattice dislocations from grain boundaries, formation of extrinsic stacking faults, and interaction of partial dislocations with twin boundaries. A combination of these deformation mechanisms and their interaction can result in considerable strain hardening before necking as well as in large post-necking deformation of nanotwinned solids, leading to their good ductility.

At the same time, many questions concerning the mechanical behaviour of nanotwinned solids remain open and need further investigation. For instance, it is not well understood how the interaction between various deformation mechanisms affect strength and ductility of nanotwinned solids. It is not clear how strain rate [35,61] and temperature [8] govern the plasticity of nanotwinned materials. The detailed mechanisms responsible for large post-necking deformation of nanotwinned solids are also yet to be detected. New experiments together with MD simulations and mechanistic modelling are required to clarify these issues.

Acknowledgements

The work was supported by the Russian Science Foundation (grant 14-29-00199), Russian Ministry of Education and Science (Zadanie 9.1964.2014K and grants 14.B25.31.0017 and MD-2893.2015.1), St. Petersburg State University research grant 6.37.671.2013 and the Russian Fund of Basic Research (grant 15-31-20095).

References

1. L. Lu, Y. Shen, X. Chen, L. Qian and K. Lu // *Science* **304** (2004) 422.
2. L. Lu, X. Chen, X. Huang, K. Lu // *Science* **323** (2009) 607.
3. T. Zhu, H. Gao // *Scr. Mater*. **66** (2012) 843.
4. I.J. Beyerlein, X. Zhang, A. Misra // *Annu. Rev. Mater. Res.* **44** (2014) 329.
5. K. Lu, L. Lu, S. Suresh // *Science* **324** (2009) 349.
6. X. Li, Y. Wei, L. Lu, K. Lu, H. Gao // *Nature* **464** (2010) 877.
7. A. Stukowski, K. Albe, D. Farkas // *Phys. Rev.* B **82** (2010) 224103.
8. A.M. Hodge, T.A. Furnish, A.A. Navid, T.W. Barbee, Jr. // *Scr. Mater.* **65** (2011) 1006.
9. Z. You, X. Li, L. Gui, Q. Lu, T. Zhu, H. Gao, L. Lu // *Acta Mater.* **61** (2013) 217.
10. Y. Tian, B. Xu, D. Yu, Y. Ma, Y. Wang, Y. Jiang, W. Hu, C. Tang, Y. Gao, K. Luo, Z. Zhao, L.-M. Wang, B. Wen, J. He, Z. Liu // *Nature* **493** (2013) 385.
11. Q. Huang, D. Yu, B. Xu, W. Hu, Y. Ma, Y. Wang, Z. Zhao, B. Wen, J. He, Z. Liu, Y. Tian // *Nature* **510** (2014) 250.
12. P. Gu, M. Dao, Y. Zhu // *Philos. Mag.* **94** (2014) 1249.
13. T.A. Furnish, A.M. Hodge // *APL Materials* **2** (2014) 046112.
14. V. Borovikov, M.I. Mendelev, A.H. King // *Philos. Mag.* **94** (2014) 2875.
15. H. Zhou, X. Li, S. Qu, W. Yang, H. Gao // *Nano Lett.* **14** (2014) 5075.
16. J. Bian, X. Niu, H. Zhang, G. Wang // *Nanoscale Research Letters* **9** (2014) 335.
17. R.J. Asaro, S. Suresh // *Acta Mater.* **53** (2005) 3369.
18. M. Dao, L. Lu, Y.F. Shen, S. Suresh // *Acta Mater.* **54** (2006) 5421
19. Z.H. Jin, P. Gumbsch, E. Ma, K. Albe, K. Lu, H. Hahn, H. Gleiter // *Scripta Mater.* **54** (2006) 1163.
20. A.J. Cao, Y.G. Wei // *J. Appl. Phys.* **102** (2007) 083511.
21. Z.M. Chen, Z.H. Jin, H.J. Gao // *Phys. Rev*. B **75** (2007) 212104.
22. A. Jerusalem, M. Dao, S. Suresh, R. Radovitzky // *Acta Mater.* **56** (2008) 4647.
23. Z.H. Jin, P. Gumbsch, K. Albe, E. Ma, K. Lu, H. Gleiter, H. Hahn // *Acta Mater.* **56** (2008) 1126.
24. L. Li, N.M. Ghoniem // *Phys. Rev.* B **79** (2009) 075444.
25. I. Shabib, R.E. Miller // *Acta Mater.* **57** (2009) 4364.
26. Y. Zhang, H. Huang // *Nanoscale Res. Lett*. **4** (2009) 34.
27. M. Chassagne, M. Legros, D. Rodney // *Acta Mater.* **59** (2011) 1456.
28. P. Gu, M. Dao, R.J. Asaro, S. Suresh // *Acta Mater.* **59** (2011) 6861.
29. Y. Wei // *Mater. Sci. Eng.* A **528** (2011) 1558.
30. L.L. Zhu, H.H. Ruan, X.Y. Li, M. Dao, H.J. Gao, J. Lu // *Acta Mater.* **59** (2011) 5544.
31. Y.T. Zhu, X.L. Wu, X.Z. Liao, J. Narayan, L.J. Kecskes, S.N. Mathaudhu // *Acta Mater.* **59** (2011) 812.
32. J. W. Yan, G. P. Zhang // *Appl. Phys. Lett.* **102** (2013) 211905.
33. X.-M. Luo, X.-F. Zhu, G.-P. Zhang // *Nat. Com.* **5** (2014) 3021.
34. T. Richeton, I. Tiba, S. Berbenni, O. Bouaziz // *Philos. Mag.* **95** (2015) 12.
35. Z. You, L. Lu // *Adv. Eng. Mater*. (2015), doi: 10.1002/adem.201500073.
36. X. Zhang, A. Misra, M. Nastasi, R.G. Hoagland. US Patent No. 7,078,108 (2006).
37. X. Zhang, A. Misra, H. Wang, M. Nastasi, J.D. Embury, T.E.Mitchell, R.G. Hoagland, J.P. Hirth // *Appl. Phys. Lett*. **84** (2004) 1096.
38. X. Zhang, H. Wang, X.H. Chen, L. Lu, K. Lu, R.G. Hoagland, K. Mishra // *Appl. Phys. Lett.* **88** (2006) 173116.

39. D. Bufford, H. Wang, X. Zhang // *Acta Mater.* **59** (2011) 93.
40. R. Niu, K. Han // *Scr. Mater.* **68** (2013) 960.
41. X. Zhang, A. Misra // *Scr. Mater.* **66** (2012) 860.
42. Y. Wei // *Phys. Rev.* B **84** (2011) 014107.
43. D. Jang, X. Li, H. Gao, J.R. Greer // *Nat. Nanotechnol.* **7** (2012) 594.
44. J. Wang, N. Li, O. Anderoglu, X. Zhang, A. Mishra, J.Y. Huang, J.P. Hirth // *Acta Mater.* **58** (2010) 2262.
45. Z.X. Wu, Y.W. Zhang, D.J. Srolovitz // *Acta Mater.* **59** (2011) 6890.
46. N.F. Morozov, I.A. Ovid'ko, N.V. Skiba // *Rev. Adv. Mater. Sci.* **37** (2014) 29.
47. Z.S. You, L. Lu, K. Lu // *Acta Mater.* **59** (2011) 6927.
48. R.E. Algra, M.A. Verheijen, M.T. Borgström, L.F. Feiner , G. Immink , W.J.P. van Enckevort, E. Vlieg, E.P.A.M. Bakkers // *Nature* **456** (2008) 369.
49. L. Wang, P. Liu, P. Guan, M. Yang, J. Sun, Y. Cheng, A. Hirata, Z. Zhang, E. Ma, M. Chen, X. Han // *Nat. Commun.* **4** (2013) 2413.
50. L. Wang, Y. Lu, D. Kong, L. Xiao, X. Sha, J. Sun, Z. Zhang, X. Han // *Acta Mater.* **90** (2015) 194.
51. T.C. Chen, Y.M. Lin, H.W. Tsai, Z.M. Wang, C.N. Liao, Y.L. Chueh // *Nanoscale* **6** (2014) 7332.
52. J. Wang, F. Sansoz, J. Huang, Y. Liu, S. Sun, Z. Zhang, S.X. Mao // *Nat. Com.* **4** (2013) 1742.
53. J. Wang, F. Sansoz, C. Deng, G. Xu, G. Han, S.X. Mao // *Nano Lett.* **15** (2015) 3865.
54. C. Deng, F. Sansoz // *Appl. Phys. Lett.* **95** (2009) 091914.
55. C. Deng, F. Sansoz // *ACS Nano* **3** (2009) 3001.
56. Z.X. Wu, Y.W. Zhang, M.H. Jhon, J.R. Greer, D.J. Srolovitz // *Acta Mater.* **61** (2013) 1831.
57. L. Liu, J. Wang, S. K. Gong, S.X. Mao // *Sci. Rep.* **4** (2014) 4397.
58. H. Zhou, S. Qu, W. Yang // *Model. Simul. Mater. Sci. Eng.* **18** (2010) 065002.
59. T. Sinha, Y. Kulkarni // *J. Appl. Phys.* **116** (2014) 183505.
60. S. Ogata, J. Li, N. Hirosaki, Y. Shibutani, S. Yip // *Phys. Rev.* B **70** (2004) 104104.
61. J. Li, J.Y. Zhang, L. Jiang, P. Zhang, K. Wu, G. Liu, J. Sun // *Mater. Sci. Eng.* A **628** (2015) 62.